Recoil ions from the β decay of ^{134}Sb confined in a Paul trap

K. Siegl,[1,2] N. D. Scielzo,[2] A. Czeszumska,[2,3,*] J. A. Clark,[4,5] G. Savard,[4,6] A. Aprahamian,[1] S. A. Caldwell,[4,6,†] B. S. Alan,[2] M. T. Burkey,[4,6] C. J. Chiara,[4,7,‡] J. P. Greene,[4] J. Harker,[4,7] S. T. Marley,[1,8] G. E. Morgan,[5,§] J. M. Munson,[3] E. B. Norman,[3] R. Orford,[4,9] S. Padgett,[2] A. Perez Galván,[4,‖] K. S. Sharma,[5] and S. Y. Strauss[1]

[1]*Department of Physics, University of Notre Dame, Notre Dame, Indiana 46556, USA*
[2]*Nuclear and Chemical Sciences Division, Lawrence Livermore National Laboratory, Livermore, California 94550, USA*
[3]*Department of Nuclear Engineering, University of California, Berkeley, California 94720, USA*
[4]*Physics Division, Argonne National Laboratory, Argonne, Illinois 60439, USA*
[5]*Department of Physics and Astronomy, University of Manitoba, Winnipeg, Manitoba R3T 2N2, Canada*
[6]*Department of Physics, University of Chicago, Chicago, Illinois 60637, USA*
[7]*Department of Chemistry and Biochemistry, University of Maryland, College Park, Maryland 20742, USA*
[8]*Department of Physics and Astronomy, Louisiana State University, Baton Rouge, Louisiana 70803, USA*
[9]*Department of Physics, McGill University, Montréal, Québec H3A 2T8, Canada*

(Received 18 September 2017; revised manuscript received 14 December 2017; published 23 March 2018)

The low-energy recoiling ions from the β decay of ^{134}Sb were studied by using the Beta-decay Paul Trap. Using this apparatus, singly charged ions were suspended in vacuum at the center of a detector array used to detect emitted β particles, γ rays, and recoil ions in coincidence. The recoil ions emerge from the trap with negligible scattering, allowing β-decay properties and the charge-state distribution of the daughter ions to be determined from the β-ion coincidences. First-forbidden β-decay theory predicts a β-ν correlation coefficient of nearly unity for the 0^- to 0^+ transition from the ground state of ^{134}Sb to the ground state of ^{134}Te. Although this transition was expected to have a nearly 100% branching ratio, an additional 17.2(52)% of the β-decay strength must populate high-lying excited states to obtain an angular correlation consistent with unity. The extracted charge-state distribution of the recoiling ions was compared with existing β-decay results and the average charge state was found to be consistent with the results from lighter nuclei.

DOI: 10.1103/PhysRevC.97.035504

I. INTRODUCTION

Radioactive isotopes confined in ion traps can be used to study a number of decay properties. By suspending ions in vacuum using only electromagnetic fields, source-scattering effects are eliminated and the recoiling nucleus is available for study. The detection of the daughter ions and β particles emerging from the trap following β decay is being exploited to study β-ν angular correlations [1–3] for tests of the standard model of particle physics and to perform β-delayed neutron spectroscopy without the challenges associated with direct neutron detection [4,5]. The direct detection of the daughter ions has allowed detailed measurements of the charge-state distributions following β decay [6,7] which can be compared with atomic-theory calculations including electron shake-off and Auger processes. In addition, the elimination of a sample backing opens up new opportunities for conversion-electron spectroscopy [8] and studies of decay branching ratios relevant for constraining matrix elements relevant to double-β decay [9,10].

In this work, the β decay of ^{134}Sb ions held in the Beta-decay Paul Trap (BPT) was studied by detecting the recoiling daughter ions and β particles in coincidence. The apparatus was built for high-precision β-decay spectroscopy and has been used to study β-decay angular correlations in the decay of ^{8}Li [11,12] and β-delayed neutron emission from fission products [4,13,14]. For the β-delayed neutron studies, the neutron-emission branching ratio $P_{\rm n}$ and energy spectrum of each species were determined from the recoil-ion spectra.

Of the isotopes produced in the heavy-mass peak following nuclear fission, ^{134}Sb has the simplest decay scheme which simplifies the interpretation of data for the β decay and subsequent propagation of the recoil ions emerging from the trapped-ion cloud. As shown in Fig. 1, the decay is dominated by the 0^- to 0^+ transition to the ground state of ^{134}Te, which previous measurements indicated has a branching ratio of 97.6(5)% [16]. Although in general, the β-ν angular-correlation coefficient $a_{\beta\nu}$ for a first-forbidden transition can depend in a complex way on the matrix elements involved [17], for a 0^- to 0^+ transition $a_{\beta\nu}$ is expected to be nearly unity [18].

*Current Address: Research Center for Nuclear Physics, Osaka University, Ibaraki, Osaka 567-0047, Japan.
†Current Address: Rigetti Computing, 775 Heinz Avenue, Berkeley, California 94710, USA.
‡Current Address: U.S. Army Research Laboratory, Adelphi, Maryland 20783, USA.
§Current Address: Department of Physics and Astronomy, Louisiana State University, Baton Rouge, Louisiana 70803, USA.
‖Current Address: Vertex Pharmaceuticals, 11010 Torreyana Rd., San Diego, California 92121, USA.

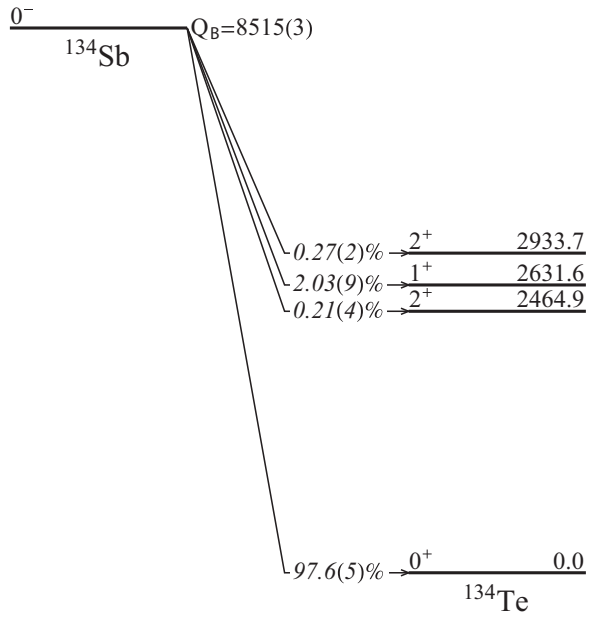

FIG. 1. The levels of ^{134}Te populated by the decay of ^{134}Sb with their published β intensities and energies in keV [15].

In addition, the β-energy spectrum for this type of transition is expected to closely resemble the allowed shape [19,20].

The 0^- to 0^+ transition in the decay of ^{134}Sb has been previously studied to understand the effects of meson-exchange currents in the nuclear medium. These currents directly affect the timelike components of the rank-zero matrix, and studies in the $A = 132$ mass region have revealed enhancements as large as 82% over the impulse approximation [21]. Analogous 0^- to 0^+ transitions in the decay of ^{92}Rb and ^{96}Y have attracted attention recently because they contribute significantly to the detected flux of high-energy neutrinos emitted from nuclear reactors.

From the β-ion coincidences collected using the BPT, the β-ν angular correlation and daughter-ion charge-state distribution were studied. There have been few measurements of charge-state distributions following β decay in this mass region and this work provides the first information on a β^- transition for an element that is not a noble gas. The results obtained here are compared with existing data on the β decay of Xe isotopes [22] as well as several other lighter noble-gas species.

II. EXPERIMENTAL TECHNIQUES

The ^{134}Sb ions ($Q_\beta = 8.515$ MeV and $t_{1/2} = 0.7$ s) were produced from the spontaneous fission of a ~100 mCi ^{252}Cf source at the Californium Rare Isotope Breeder Upgrade (CARIBU) facility at Argonne National Laboratory (ANL). CARIBU also provides a 7^- isomer, ^{134m}Sb ($Q_\beta = 8.794$ MeV and $t_{1/2} = 10$ s) and this isomer is produced with an intensity of about twice that of ^{134}Sb. The half-lives for ^{134}Sb and ^{134m}Sb used in this work are from a recent measurement at CARIBU [23], although updating the half-lives had minimal impact on the ^{134}Sb results presented in this paper. The β decay of ^{134m}Sb has a significantly more complicated decay pattern than that of ^{134}Sb and has a negligible decay branch directly to the ground state of ^{134}Te. Instead, multiple excited states are populated, including a state at 1691 keV which has a half-life of 164 ns and deexcites by a highly converted transition to the 1576 keV state.

The ^{252}Cf fission fragments were thermalized by using a large helium-filled gas catcher and extracted as a continuous low-energy beam of singly charged ions by using a combination of gas flow and electric fields [24]. The beam was sent through an isobar separator [25] operated with a mass resolution of $\frac{M}{\Delta M} \approx 15\,000$ to isolate ^{134,134m}Sb. A radio-frequency-quadrupole (RFQ) buncher containing a small amount of helium gas was used to accumulate, cool, and bunch the beam [24]. These ion bunches were delivered through an electrostatic beam line to the BPT where they were collected and held for the decay measurements.

The mass selectivity of the ion delivery was not sufficient to separate ^{134}Sb from ^{134m}Sb, so instead measurements were made under two different accumulation and measurement cycles which took advantage of the order-of-magnitude difference in radioactive half-lives to collect data sets with significantly different decay contributions from the two species. A first set of measurements used a 0.6 s accumulation time in the RFQ buncher, which was better matched for the shorter-lived ^{134}Sb decay and will be referred to as the "^{134}Sb-optimized measurement cycle." Ten of these bunches were collected in the BPT (for a total measurement time of 5.9 s), followed by ejection of the ions from the BPT to measure any remaining backgrounds over the subsequent 4.3 s. This measurement cycle was run for 32.6 h.

Data were collected by using a second measurement cycle, better suited for the decay of ^{134m}Sb, with ions accumulated for 6 s in the RFQ buncher, a buildup of ions in the BPT over 59.9 s, followed by a background measurement of 30.1 s. This will be referred to as the "^{134m}Sb-optimized measurement cycle." This measurement cycle was run for 6.1 h.

In the ^{134}Sb-optimized measurement cycle, the number of β decays from trapped ^{134}Sb and ^{134m}Sb ions was expected to be similar, while for the ^{134m}Sb-optimized measurement cycle, the ^{134m}Sb decay contributed approximately 90% of the decays from trapped ions. The data collected with the ^{134m}Sb-optimized measurement cycle were used to subtract the ^{134m}Sb contributions from the data collected with the ^{134}Sb-optimized measurement cycle.

The BPT is a linear RFQ ion trap with electrodes designed to allow the trapped-ion cloud to be surrounded by an array of radiation detectors [26]. In this work, the BPT was instrumented with a detector array consisting of two ΔE-E plastic scintillator telescopes, two microchannel-plate (MCP) detectors, and two high-purity germanium (HPGe) detectors to detect the β particles, recoil ions, and γ rays, respectively, emitted following β decay. A cross-sectional view of the trap and the detector array is shown in Fig. 2.

The four sets of thin electrode plates used to confine the ions come within 11 mm of the trap center and were each divided into three segments along the beam axis. A radio-frequency potential with a peak-to-peak voltage $V_{pp} = 190$ V at a frequency of 310 kHz was applied to the electrode plates

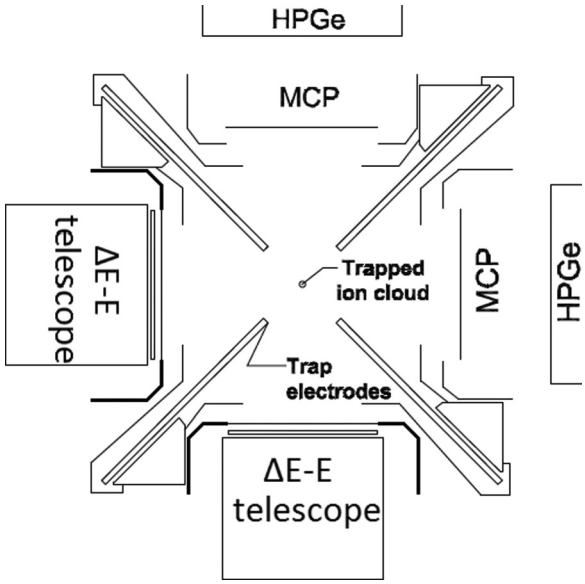

FIG. 2. A cross-sectional view of the BPT and the detector array used in this work, not to scale. The beam axis points out of the page, and the detectors are identified according to their positioning relative to this axis. In the left and bottom positions are the two ΔE-E plastic-scintillator detectors used for β-particle detection, and in the right and top positions are two MCP detectors and two HPGe detectors used for recoil-ion and γ-ray detection, respectively.

to confine the ions radially. The voltage was directly measured by using a high-voltage probe and contributions from higher harmonics at 620 and 930 kHz were found to contribute with amplitudes less than 10% of the amplitude of the primary frequency. In the axial direction, the ions were confined by dc voltages of +20, −17, and +20 V applied to the segments. The trap volume was suffused with helium buffer gas at a pressure of $\sim 5 \times 10^{-5}$ Torr to cool the trapped ions and minimize the spatial extent of the ion cloud. Ion bunches were loaded into the trap by lowering the dc potential on the entrance segments, while maintaining a ∼5 V electrostatic valley needed to retain the previously trapped ions.

The ΔE-E plastic-scintillator detector telescopes, located 105 mm from the trap center in the bottom and left detector positions, each had a 1-mm-thick, 10.6-cm-diameter ΔE detector positioned in front of a 10.2-cm-thick, 13.3-cm-diameter E detector capable of stopping all the β particles emitted from ion decays. The light from the ΔE detector was piped to two 3.8-cm-diameter photomultiplier tubes (PMTs) using light-guide strips wrapped in thin specular reflectors. The E-scintillator cylinder wall was coated in a layer of diffuse reflector paint and attached directly to a 12.7-cm-diameter PMT. Each detector telescope was supported in a vacuum chamber held at a pressure below 10^{-3} Torr, which was separated from the vacuum environment of the ion trap by a 10-μm-thick aluminized Kapton window.

The β particles were identified by energy deposition in the ΔE detector. Measurements of the energy deposition from ^{134}Sb decays and from a spectroscopy-grade ^{207}Bi conversion-electron source indicated that the ΔE detector energy threshold for β particles was approximately 70 keV. This thin detector has only a ∼1% intrinsic detection efficiency for γ rays and neutrons.

The MCP detectors each consisted of a resistance-matched pair of MCPs arranged in a chevron configuration with a resistive anode. The right and top MCP detectors each had nominal active areas of 50.3×50.3 mm^2 and were located 52.9(3) and 52.5(3) mm, respectively, from the center of the trap and 4.5 mm behind grounded, 89%-transmission grids. The front surface of the MCP was biased to approximately −2.5 kV to accelerate the recoiling daughter ions (which all have charge states of 2^+ or greater) to energies of at least 5 keV and impact angles within a few degrees of the detector normal. The MCP timing resolution was <1 ns and the recoil-ion hit locations were reconstructed from the charge division at the four corners of the resistive anode [27]. The position calibration was obtained prior to the data collection by imaging the pattern from a mask placed on the MCP by using a ^{238}Pu α source. A fiducial-area cut of 46.0×46.0 mm^2 was used to select events as the position for these events could be reconstructed within about 0.1 mm. For a few percent of the events, the pulse amplitude on one of the corners was just beyond the range of the ADC, and the hit position had to be reconstructed from the charge collected on the other three corners.

For recoil ions with kinetic energies above a few keV, the pulse-height distribution (PHD) of the MCP detector output is well described by a Gaussian distribution [6,28,29] and the intrinsic detection efficiency is expected to be nearly independent of energy [30,31] with only a small fraction of the PHD falling below the electronic threshold. A detailed analysis of the fraction of the PHD below threshold was performed [14] in a manner similar to the efficiency corrections in Refs. [6,29] for the two detectors as a function of hit location and ion-impact energy. The results indicated that about 1.6% of the PHD from the right MCP detector and 16% of the PHD for the top MCP detector, which had a lower gain, was expected to be below threshold.

Two single-crystal p-type HPGe detectors, with relative efficiencies of 80% and 140%, were placed behind the top and right MCP detectors, respectively. The MCP-detector housings were specially designed to be compact to fit between the electrodes of the BPT and to allow HPGe detectors to be brought within 10 cm of the trapped ion cloud. The efficiencies of the HPGe detectors were determined by using sealed sources of ^{60}Co, ^{133}Ba, ^{137}Cs, and ^{152}Eu which had activities calibrated to within 1.5%–2.5% (at 1σ).

The data acquisition was triggered when a signal from any detector rose above the constant-fraction-discriminator threshold. For every trigger, a 20-μs coincidence window was opened to record the amplitude and timing of all the detector signals. The length of the window was selected to allow sufficient time for all the recoil ions to be detected. The nonparalyzable dead time was determined to be 142 μs. The timing of the trigger relative to the measurement cycle and the phase of the applied rf field was also recorded. The time of flight (TOF) for recoil ions was determined with a full width at half maximum (FWHM) timing resolution of 3 ns from coincidences between a ΔE plastic scintillator and a MCP detector.

III. ANALYSIS

The first step of the analysis was to isolate the contributions from the decay of ^{134}Sb from those of ^{134m}Sb by taking the appropriate combination of the data collected under the ^{134}Sb-optimized and ^{134m}Sb-optimized measurement cycles. The results obtained for the decay of ^{134}Sb were then compared with simulations of the β decay occurring within the ion cloud and the subsequent propagation and detection of the emitted particles within the apparatus. First, the charge-state distribution was constrained by studying the rf-phase dependence of the β-ion coincidence rate. Once values for the charge-state distribution were obtained, the ion-cloud distribution and then properties of the 0^- to 0^+ transition such as the β-ν correlation and the branching ratio could be studied. Finally, with the decay and ion-cloud properties established, the intrinsic detection efficiencies of the MCP detectors were determined from comparisons of the number of detected β-ion coincidences with the predictions from simulations. The steps of the analysis are described in detail in the following sections.

A. Isolating the ^{134}Sb decay contributions

The relative contributions from the decay of trapped ^{134m}Sb ions in the two measurements were determined from the buildup and decay of several decay signatures. The decay of ^{134m}Sb emits β particles, several high-intensity γ rays, and conversion electrons (CEs). Comparing the β singles, γ-ray singles spectrum, β-γ coincidences, β-ion coincidences, and β-CE coincidences allowed the quantification of the relative amount of ^{134m}Sb in the two sets of data. Only the results from the fully independent β-singles and γ-ray-singles spectra were used here, although the coincidence methods agreed with these results.

The determination of the trapped ^{134m}Sb activity is complicated by backgrounds that arise from ions that are delivered to the BPT but end up unconfined, either because they are not initially captured by the electric fields or they escape the trap during the measurement cycle, due to effects such as charge exchange with contamination in the buffer gas. These unconfined ions can potentially be distributed around the interior of the vacuum chamber. The background segment of the measurement cycle allows the assessment of these contributions.

The time dependence of the buildup and decay profile of the β- and γ-ray singles depends on the half-lives of ^{134}Sb and ^{134m}Sb, the composition of the ion beam delivered to the BPT, the relative detection efficiencies of the trapped and distributed decays, and the rate of ions escaping the BPT. The daughter ^{134}Te has a radioactive half-life of 41.8(8) min and therefore provides a background contribution which is nearly constant in time. The relative detection efficiencies and the relative rates can be well determined from the time dependence of the β singles during the measurement, and a systematic uncertainty was assigned to account for the uncertainty in the half-lives and charge-exchange effect [13].

The 1279, 706, and 297 keV γ rays emitted in the decay of ^{134m}Sb were used to determine the relative number of decays from trapped ^{134m}Sb ions in the two data sets. As with the β-singles analysis, the background from ^{134m}Sb activity outside of the ion cloud was taken into account by using the number of counts of each γ ray in the background period of the trap cycle. The 1279 keV γ-ray result required an additional correction of $\sim$3% because this γ ray is also present in the decay of ^{134}Sb at an absolute intensity of 1.1(5)% [15].

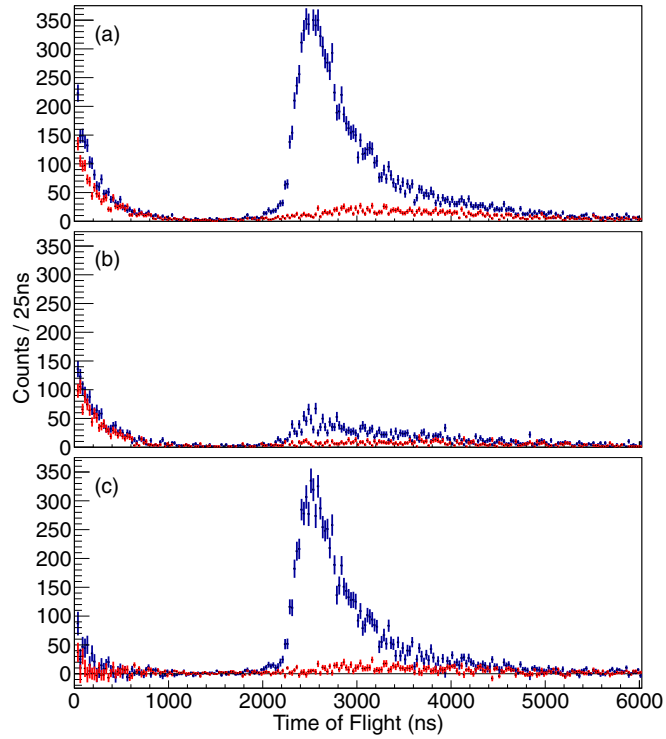

FIG. 3. Time-of-flight spectrum for β-ion coincidences for (a) the ^{134}Sb-optimized measurement cycle, (b) the ^{134m}Sb-optimized measurement cycle scaled to have the same ^{134m}Sb decay contribution as in the ^{134}Sb-optimized measurements (as described in the text), and (c) the ^{134}Sb spectrum obtained by subtracting the ^{134m}Sb contribution. The data collected with the ΔE-MCP detector pairs separated by 180° (left ΔE with right MCP and bottom ΔE with top MCP) are shown in blue while the data for detector pairs separated by 90° (left ΔE with top MCP and bottom ΔE with right MCP) are shown in red.

The ratio of the decays of trapped ^{134m}Sb ions in the ^{134}Sb-optimized measurement cycle to that of the ^{134m}Sb-optimized measurement cycle was determined to be 1.399(74) and 1.562(93) from the analysis of the β- and γ-ray singles rates, respectively, resulting in an average value of 1.462(58). This ratio is needed to isolate the ^{134}Sb decay signatures. The TOF distributions from the two measurements and the isolated ^{134}Sb result are shown in Fig. 3.

The number of β-ion coincidences for each detector pair, shown in Table I, was determined after subtracting off accidental coincidences determined from coincidences with TOF between 15 and 20 μs. The ratio of the coincidences detected with the ΔE-MCP detector pairs separated by 180°, $n_{\beta r}(180°)$, and the detector pairs separated by 90°, $n_{\beta r}(90°)$,

$$R_{180/90} = \frac{n_{\beta r}(180°)}{n_{\beta r}(90°)}, \tag{1}$$

TABLE I. Number of β-ion coincidences detected by using the different ΔE-MCP detector combinations for the data acquired in the ^{134}Sb optimized (0.6 s accumulation time), and the ^{134m}Sb optimized (6 s accumulation time) measurement cycles as well as the ^{134}Sb isolated coincidences as described in the text.

Coincidence		Accumulation Time		^{134}Sb
ΔE	MCP	0.6 s	6 s	Isolated
Left	Top	863(38)	282(24)	450(54)
Bottom	Right	1140(47)	390(28)	570(66)
Bottom	Top	5571(80)	928(34)	4214(109)
Left	Right	7010(92)	1172(39)	5297(128)
$R_{180/90}$		6.28(20)	3.12(19)	9.33(80)

serves as an important observable that needs to be reproduced by any simulation of the ^{134}Sb β decay. The experimentally measured value of $R_{180/90} = 9.33(80)$ in Table I provides a constraint that is sensitive to $a_{\beta\nu}$ and the decay branching ratios and less sensitive to other decay properties such as the charge-state distribution.

The TOF structure present below 1000 ns arises from ^{134m}Sb decays in which the β particle triggers the ΔE detector and a CE emitted from the 1691 keV excited state in ^{134}Te triggers the MCP detector. This excited state has a half-life of 164.1 ns and therefore delays the CE emission, resulting in a nearly exponential-decay feature extending out to ~1000 ns. The subtraction of the trapped ^{134m}Sb contribution greatly reduces the number of β-CE coincidences, but is not expected to completely eliminate them because of coincidences from ^{134m}Sb activity remaining outside of the ion cloud.

B. β-decay simulations

The TOF and β-energy distributions for β-ion coincidences were compared with simulations of the ^{134}Sb decay and subsequent propagation and detection of the decay radiation and recoil ions. The β-decay kinematics were simulated by using an event generator originally developed in Ref. [32] and adapted to simulate fission-product decays in Ref. [4]. The β and ν energy distributions for each transition were assumed to have an allowed spectral shape and permitted to have any value of $a_{\beta\nu}$ from -1 to $+1$. For this work the event generator was further adapted to allow for decays populating multiple excited levels, with the deexcitation pathways taken from the Reference Input Parameter Library (RIPL-3) [33], with γ rays and CEs emitted isotropically. The recoil of the daughter nucleus was then determined from the momentum imparted by all of the emitted particles. The decays are distributed spatially with a Gaussian distribution in all three dimensions centered at the electric-field minimum, and uniformly in time over the trap rf period.

The β particle and any accompanying γ rays and CEs were propagated through a GEANT4 [34–36] simulation of the ion-trap and detector-array geometry to identify decays which deposit energy in the ΔE and E plastic scintillators. Recoiling ions with charge states of 2^+, 3^+, and 4^+ were propagated through the time-varying electric field of the BPT by using the ion-optics program SimIon [37]. For each ion that hit an MCP detector, the TOF, hit position, impact energy, and rf phase at the time of the decay were recorded. The β-ion coincidences were then identified from decays in which the total energy deposited in a ΔE detector was larger than the energy threshold and the ion impacted the fiducial area of either MCP detector. In addition, an efficiency correction was applied to account for the fraction of the PHD lost to the electronic threshold [14].

C. Charge-state distribution

The recoil-ion trajectories were significantly influenced by the electric field as the maximum energy of 290 eV, imparted by the β decay, was comparable to the voltages applied to the BPT electrodes. As a result, the likelihood of an ion striking one of the MCP detectors and the TOF distribution of the β-ion coincidence were dependent on the ion charge state. However, unlike in other ion-trap experiments where an electric field guides recoil ions into an MCP detector and separates the charge states by TOF [6], the acceleration region for this experiment was only the last 4.5 mm in front of the MCP, which was insufficient for ions of each charge to arrive in distinct TOF windows.

Instead, the charge-state distribution was inferred from the rf-phase dependence of the β-ion coincidence rate. The ion charge state influenced the magnitude of the change in the coincidence rate as a function of the rf phase, with higher charge states having a greater reduction in rate at certain values of the rf phase. Simulations for the 2^+, 3^+, and 4^+ charge states are shown in Fig. 4. As the contribution of each charge state cannot be independently determined, a separate constraint is necessary. Previous results from a variety of atomic systems are consistent with the charge-state distribution following β decay decreasing with increasing charge state [6,22,38,39]. Therefore, a geometric progression in the probability of higher

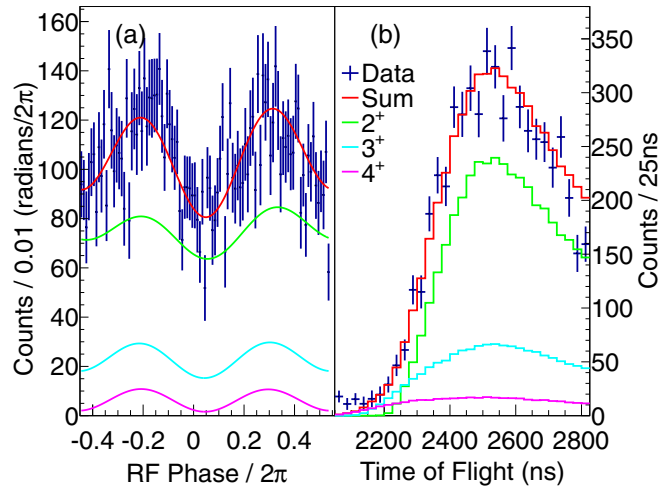

FIG. 4. (a) The rf-phase dependence of β-ion coincidences from the decay of ^{134}Sb. The best fit (red) from simulations consists of the sum of 2^+ (green), 3^+ (cyan), and 4^+ (magenta) contributions. (b) The resulting TOF spectra from the charge-state distribution determined from the rf phase, confined to 2000 to 2800 ns to illustrate the low TOF behavior of the charge states.

charge states was adopted as a constraint. The result is a simple charge-state-distribution model including the 2^+, 3^+, and 4^+ charge states where each charge-state abundance is reduced by a constant multiplicative factor (fit to best reproduce the data) from the one before it. From a fit to this model the mean charge state following the β decay of ^{134}Sb was determined to be +2.42(6). This method of determining the charge-state distribution gave results nearly independent of the details of the decay properties as long as they were adjusted to give a value for $R_{180/90}$ consistent with the measured value.

Although the actual charge-state distribution following β decay can extend beyond 4^+, the higher charge states are typically produced with decreasing probability [6,22] and the truncation of the charge state has only a minimal effect on the results. Given the simplicity of the approach, it was deemed unnecessary to extend the charge-state distribution beyond 4^+. For the TOF distribution, the largest effect of the charge state was on the rising edge between 2100 and 2300 ns as can be seen in Fig. 4(b). The β-ion coincidences with TOF below 2100 ns, absent in the simulation, are consistent with 2%–3% of the decays resulting in ions with higher charge states. A number of these ions gain energy from the rf fields and arrive sooner at the MCP detector. Charge states greater than 6^+ would contribute to this TOF region, as would ions that decay into states that deexcite through CE emitting transitions, which can result in very high charge states [22].

D. Ion-cloud spatial distribution and location

The spatial extent of the ion cloud influences the shape of the peak of the TOF distribution between 2000 and 2600 ns, as can be seen in Fig. 5. Once the charge-state distribution has been determined from the rf-phase dependence of the β-ion coincidence rate, the size of the ion cloud can be estimated. An ion cloud with a Gaussian distribution of 1 mm at FWHM (assumed to be identical in all three spatial dimensions) was found to best match the data. In this simulation, the decay scheme from Ref. [16] with nearly all decays to the ground state and a value of $a_{\beta\nu} = 1$ for this transition were used, although allowing for either $a_{\beta\nu} < 1$ or additional decays to as-of-yet unknown excited states has minimal impact on the determination of the ion-cloud extent.

The timing of the half-maximum in the rising edge of the TOF distribution depends primarily on the distance between the ion cloud and the MCP detectors and the Q_β of the decay. The rf electric fields shift this timing by only 3% and both the rf and dc electric fields were precisely accounted for in the simulations. Agreement between the data and simulations was obtained when using MCP detector distances of 53.0(5) mm in the simulations and this value was used in the analysis. These results were consistent with the distances of 52.5(3) and 52.9(3) mm determined from the physical measurement of the placement of the detectors and electrodes.

E. 0^- to 0^+ transition properties

The experimental results for $R_{180/90}$, together with the TOF and β-energy spectra for β-ion coincidences, were compared with simulations to understand properties of the 0^- to 0^+ transition to the ground state of ^{134}Te. The value of $R_{180/90} = 9.33(80)$ from this measurement was inconsistent with the value of 12.5 expected from simulations based on the previously available decay properties [16] when $a_{\beta\nu} = 1$ was used for the 0^- to 0^+ transition (which had a 97.6% branching ratio). Two approaches were pursued to explain this surprising result.

The first method was to assume that the known decay properties were complete and to adjust the $a_{\beta\nu}$ for the 0^- to 0^+ transition in order to match $R_{180/90}$. This approach yielded a value of $a_{\beta\nu} = 0.47(16)$. The resulting TOF spectrum also agrees well with the data as, shown in Fig. 6.

The second method was to fix $a_{\beta\nu} = 1$ for the 0^- to 0^+ transition and to allow for decay feeding to highly excited states,

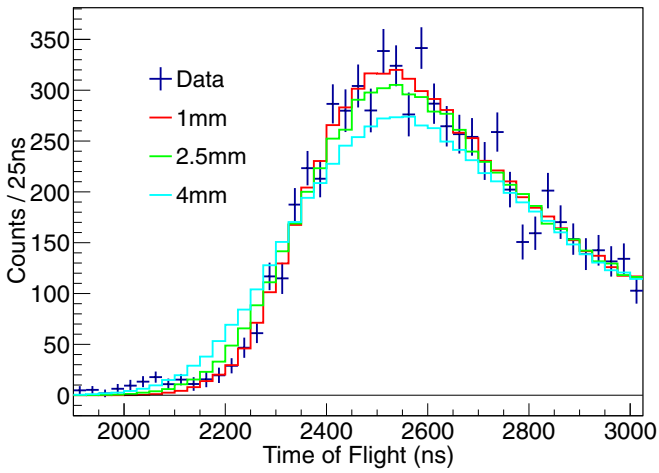

FIG. 5. The rising edge of the ^{134}Sb decay TOF compared with three simulated cloud sizes, labeled by the FWHM of the Gaussian distribution used. The 1 mm (red) simulation is scaled to match counts between 2400–2600 ns, and the 2.5 mm (green) and 4 mm (cyan) are shown with the same number of β-ion coincidences as the 1 mm simulation.

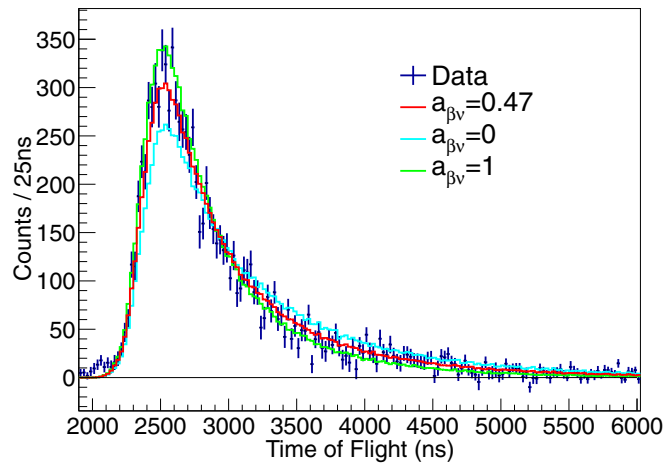

FIG. 6. The measured ^{134}Sb TOF spectrum compared with simulations using the decay scheme in Ref. [16] with different $a_{\beta\nu}$ values. The value which matches $R_{180/90} = 9.33$ from the data is $a_{\beta\nu} = 0.47$ and the resulting TOF distribution is shown in red. The TOF spectra for $a_{\beta\nu} = 0$ (cyan) and $a_{\beta\nu} = 1$ (green) are also shown and result in $R_{180/90}$ values that are inconsistent with the data.

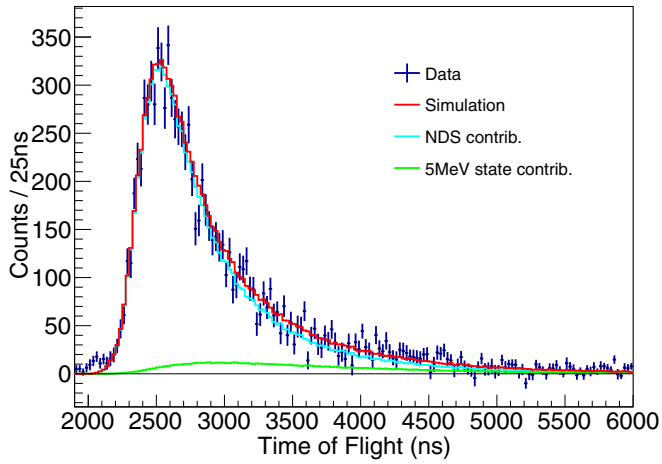

FIG. 7. The TOF spectrum for β-ion coincidences compared with simulations (red) which include the decay scheme from the Nuclear Data Sheets [16] with $a_{\beta\nu} = 1$ (cyan) and a single fictitious allowed Gamow–Teller transition with $a_{\beta\nu} = -1/3$ to a 5 MeV excited state (green) which decays directly to the ground state by a single γ ray.

which may have escaped observation in previous experiments. To allow for this possibility, allowed Gamow–Teller transitions (with $a_{\beta\nu} = -1/3$) to fictitious excited states between 4 and 6 MeV that decay to the ^{134}Te ground state by emitting a single γ ray were simulated. These decays were chosen to approximate any decay branches to high-lying states for which the nuclear recoil was less dependent on the β-particle momentum. For example, for the 5 MeV excited state, $R_{180/90} = 1.9$ and therefore 17.2(52)% of the decays proceeding by this transition could explain the data. The effects of this additional decay branch on the TOF spectrum and the comparison to data are shown in Fig. 7.

F. Intrinsic efficiency of microchannel-plate detector

The intrinsic efficiency of the MCP detector, ϵ_{MCP}, can be determined from the data, and this is necessary to determine the recoil-ion detection efficiency used in β-delayed neutron branching-ratio measurements [4,13,14]. This efficiency is the likelihood that a recoiling ion which originated in the ion cloud and reached the MCP detector face will deposit charge on the resistive anode. For the recoiling ^{134}Te ions, ϵ_{MCP} was determined by comparing the data to the simulation ("sim") results by using the relation

$$\left(\frac{n_{\beta r}}{n_\beta}\right)_{\mathrm{data}} = \left(\frac{n_{\beta r}}{n_\beta}\right)_{\mathrm{sim}} \epsilon_{\mathrm{MCP}}, \qquad (2)$$

where $n_{\beta r}$ is the number of detected β-ion coincidences, and n_β is the number of detected β particles from the trapped ions. The simulation results include the small, impact-energy-dependent loss of ion counts due to MCP pulses which fall below the electronic threshold. This correction is described in detail in Ref. [14].

The experimental results for ϵ_{MCP} determined from $(\frac{n_{\beta r}}{n_\beta})_{\mathrm{data}}$ are shown in Table II for the various detector combinations.

The value of ϵ_{MCP} obtained using the two sets of decay properties described in Sec. III E only differed by ∼1.2%, and this served as an estimate of the systematic uncertainty associated with incomplete knowledge of the decay. The systematic uncertainty from the charge-state distribution determination and the β-particle scattering were 1.3% and 0.6%, respectively. As shown in Table II the total uncertainty was dominated by the statistical uncertainty, which incorporates the uncertainty associated with the isomer subtraction.

TABLE II. Ratio of β-ion coincidences to total number of detected β particles in data and simulation, with extracted MCP detector intrinsic efficiency.

Coincidence		$n_{\beta r}/n_\beta$ (%)		ϵ_{MCP} (%)	σ_{stat}	σ_{sys}
ΔE	MCP	Data	Sim.			
Left	Top	0.60(8)	1.89(3)	31.5	4.0	0.5
Bottom	Right	0.71(9)	2.27(3)	31.1	3.8	0.8
Bottom	Top	5.2(2)	18.0(1)	29.0	1.3	0.6
Left	Right	7.0(3)	20.9(1)	33.6	1.4	0.7
			Top	29.3	1.2	0.6
			Right	33.3	1.3	0.7

The value of ϵ_{MCP} is expected to be less than unity because of the 60% open area ratio of the MCP channels [31] and the loss of ions passing through the two 89%-transmission grids located between the ion-cloud region and the MCP detector. The electric field of 5.5 kV/cm in front of the MCP detectors used to accelerate ions for detection also served to strip away electrons from the detector front surface. Offline analysis using an α-particle source confirmed that ϵ_{MCP} decreased by 10%–20% at the electric fields used in this experiment. The magnitude of this effect on the detection of keV-energy heavy ions may be different than for MeV-energy α particles.

IV. DISCUSSION

A. Charge-state distribution

The daughter-ion charge-state distribution determined following the decay of ^{134}Sb ions is the first for the β^- decay of an element other that a noble gas. The closest atomic system with which it can be compared is the β^- decay of ^{133}Xe to ^{133}Cs [22]. In this decay, the mean electron loss for the β-decay component was found to be 0.33, a value close to the 0.42(6) found for ^{134}Sb ions. The results from this and all other measurements of charge-state distributions following the β^- decay are shown in Table III. These results show that, with the exception of the one-electron system of ^{6}He^{1+} [7], the mean electron loss ranges from 0.19 to 0.42 and is consistent with the result obtained here. This entire variation of the mean electron loss would result in only a 10% spread in the average daughter-ion charge state following trapped-ion decay and provides some insight as to what can be expected following the decay of other nuclides.

B. 0^- to 0^+ transition properties

For a 0^- to 0^+ transition, only the two matrix elements which arise from the timelike and spacelike components of

TABLE III. Mean atomic electron loss following β decay for noble gases compared with this work.

Species	Parent charge	1 e^- Prob.	Mean e^- loss
^{6}He [40]	0	0.104(2)	0.188(2)
^{6}He [7]	1^+	0.0233(4)	0.0233(4)
^{23}Ne [41]	0	0.175(1)	0.250(3)
^{35}Ar [6]	1^+	0.172(4)	0.362(23)
^{41}Ar [38]	0	0.125(8)	0.26(2)
^{85}Kr [39]	0	0.109(2)	0.42(3)
^{133}Xe [22]	0	0.08[a]	0.33[a]
^{134}Sb[b]	1^+	0.243[c]	0.42(6)[c]

[a]Charge-state uncertainties are not quoted after removing CE effect.
[b]This work.
[c]Result from a simple model which assumes a decreasing geometric progression truncated at 4^+.

the axial current contribute to the decay [42] and are denoted here as ξ_0 and ω, respectively, as in Ref. [18]. The β-ν angular correlation can then be expressed as

$$a_{\beta\nu}(W) = \frac{{\xi_0}^2 - \frac{1}{9}\omega^2}{{\xi_0}^2 + \frac{1}{9}\omega^2 - \frac{2}{3}\xi_0\omega\frac{m_e}{W}}, \quad (3)$$

where W and m_e are the total energy and mass, respectively, of the β^- particle and terms dependent on αZ are ignored [18]. The matrix elements for the ^{134}Sb transition were calculated in Ref. [21] and ξ_0 was determined to be much larger than ω, in agreement with the prediction of Siegert's theorem [43]. As a result, $a_{\beta\nu}$ must be nearly unity. From Eq. (3), a value of $a_{\beta\nu} = 0.47$ would require $\omega \simeq 1.8 \times \xi_0$ and therefore cannot be the explanation for the observed value of $R_{180/90}$.

The presence of additional β-decay feeding to high-lying states provided the best explanation for the β-ion coincidence data and β-energy spectrum. The addition of transitions to these excited states better described features of the β-energy spectrum below 5 MeV. Excited states in the 4–6 MeV energy range were examined, with a single transition to a 5 MeV state with an intensity of 17.2(52)% best matching the data. The addition of this transition best described the shape of the β-energy spectrum, as shown in Fig. 8, and reduced the branching ratio to the ground state to 80.4(52)%. The total intensity to excited states was not sensitive to the exact excitation energy of the added transition as results obtained for excited states in the 4–6 MeV energy range were well within the 1-σ uncertainty. As ^{134}Te is a relatively heavy and neutron-rich nucleus, the additional decay strength to highly excited states is likely due to a plethora of weak allowed transitions to 1^- states from the decay of ^{134}Sb that were missed in previous experiments, a phenomenon that has come to be known as the "pandemonium effect" [44].

Recent measurements by total absorption spectroscopy of the decay of ^{92}Rb, a light fission peak nucleus also dominated by a 0^- to 0^+ ground-state transition, observed similarly isolated additional β-decay strength to states between 4.5 and 5.5 MeV [45,46]. The 0^- to 0^+ was determined to have an intensity of about 90%, reduced from the previously determined 95.2(7)% [47].

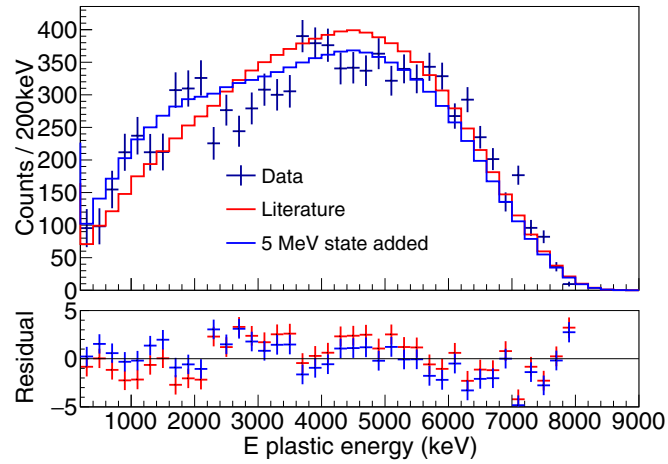

FIG. 8. The β-energy spectrum for β-ion coincidences compared with simulations which include the decay scheme from the Nuclear Data Sheets [16] with $a_{\beta\nu} = 1$ (red) combined with a single fictitious allowed Gamow–Teller transition with $a_{\beta\nu} = -1/3$ to a 5 MeV (blue) excited state which decays directly to the ground state by a single γ ray, scaled to match counts above 200 keV.

V. CONCLUSIONS

The decay of ^{134}Sb was studied by detecting the β particles and recoiling daughter ions which emerge from the BPT in coincidence. By holding ions in vacuum using only electric fields, the charge-state distribution following β decay and the properties of the dominant 0^- to 0^+ transition in the β decay of ^{134}Sb to ^{134}Te were investigated. Utilizing two measurements with different collection and measurement cycles, the ^{134}Sb decay signatures were isolated from those of the decay of ^{134m}Sb, even though ^{134m}Sb was produced more abundantly by ^{252}Cf fission.

The charge-state distribution was studied by analyzing rf-phase dependence of the β-ion coincidence rate. By using a simplifying assumption that the charge-state distribution follows a geometric progression, the mean electron loss was determined and found to be similar to the results from other β-decay experiments [6,22,38–41].

The β-ion coincidence rate observed at the different detector pairs were incompatible with the predictions based on previous measurements of the decay scheme and a value of $a_{\beta\nu} = 1$ for the 0^- to 0^+ transition. To explain this discrepancy, an additional 17.2(52)% of the β-decay transitions must populate highly excited states in the daughter ^{134}Te nucleus. These additional transitions also improve the agreement between the measured and simulated β-energy spectra for β-ion coincidences. Without any additional transitions, $a_{\beta\nu}$ must otherwise be significantly smaller than unity, in disagreement with the prediction of first-forbidden β decay theory. Additional measurements would be of interest to investigate the excited-state transitions more precisely.

In addition, the efficiency of the MCP detectors for the 5 keV ^{134}Te recoil ions was determined in a way that was nearly independent of the details of the β-decay scheme as long as the observed value for $R_{180/90}$ was reproduced. An *in situ* measurement of the MCP efficiency is useful for the analysis of β-delayed neutron emission measurements performed with the BPT.

The β-decay simulation and methodology for analyzing recoil-ion properties described here can also be used to interpret the data collected for other nuclides and will be useful for studying decays for which there is significantly less information available. Future measurements will benefit from the improved intensity [48] and purity [49] of CARIBU ion beams and would allow the study of isotopes further from stability.

ACKNOWLEDGMENTS

This material is based upon work supported by the National Science Foundation, under Grant No. PHY-1419765 (University of Notre Dame); Department of Energy, National Nuclear Security Administration, under Award No. DE-NA0000979 (NSSC), No. DE-AC52-07NA27344 (LLNL), No. DE-NA0002135(SSGF); Office of Nuclear Physics Contract DE-AC02-06CH11357 (ANL), and grants DE-FG02-94ER40834 (University of Maryland), DE-FG02-98ER41086 (Northwestern University); Nuclear Energy University Program, under Project No. 13-5485 (University of California, Berkeley); Louisiana Board of Regents Research Competitiveness Subprogram LEQSF(2016-19)-RD-A-09; NSERC (Canada), Application No. SAPPJ-2015-00034 (CPI 1199136).

[1] X. Fléchard, E. Liénard, A. Méry, D. Rodriguez, G. Ban, D. Durand, F. Duval, M. Herbane, M. Labalme, F. Mauger, O. Naviliat-Cuncic, J. C. Thomas, and P. Velten, Phys. Rev. Lett. **101**, 212504 (2008).
[2] X. Flécard *et al.*, J. Phys. G **38**, 055101 (2011).
[3] S. Van Gorp, M. Breitenfeldt, M. Tandecki, M. Beck, P. Finlay, P. Friedag, F. Gluck, A. Herlert, V. Kozlov, T. Porobic, G. Soti, E. Traykov, F. Wauters, C. Weinheimer, D. Zákoucký, and N. Severijns, Phys. Rev. C **90**, 025502 (2014).
[4] R. M. Yee, N. D. Scielzo, P. F. Bertone, F. Buchinger, S. Caldwell, J. A. Clark, C. M. Deibel, J. Fallis, J. P. Greene, S. Gulick, D. Lascar, A. F. Levand, G. Li, E. B. Norman, M. Pedretti, G. Savard, R. E. Segel, K. S. Sharma, M. G. Sternberg, J. Van Schelt, and B. J. Zabransky, Phys. Rev. Lett. **110**, 092501 (2013).
[5] N. D. Scielzo *et al.*, Nucl. Data Sheets **120**, 70 (2014).
[6] C. Couratin, X. Fabian, B. Fabre, B. Pons, X. Fléchard, E. Liénard, G. Ban, M. Breitenfeldt, P. Delahaye, D. Durand, A. Méry, O. Naviliat-Cuncic, T. Porobic, G. Quéméner, D. Rodriguez, N. Severijns, J.-C. Thomas, and S. Van Gorp, Phys. Rev. A **88**, 041403(R) (2013).
[7] C. Couratin, P. Velten, X. Fléchard, E. Liénard, G. Ban, A. Cassimi, P. Delahaye, D. Durand, D. Hennecart, F. Mauger, A. Méry, O. Naviliat-Cuncic, Z. Patyk, D. Rodriguez, K. Siegień-Iwaniuk, and J. C. Thomas, Phys. Rev. Lett. **108**, 243201 (2012).
[8] J. Rissanen *et al.*, Eur. Phys. J. A **34**, 113 (2007).
[9] A. Lennarz, A. Grossheim, K. G. Leach, M. Alanssari, T. Brunner, A. Chaudhuri, U. Chowdhury, J. Crespo López-Urrutia, A. T. Gallant, M. Holl, A. A. Kwiatkowski, J. Lassen, T. D. Macdonald, B. E. Schultz, S. Seeraji, M. C. Simon, C. Andreoiu, J. Dilling, and D. Frekers, Phys. Rev. Lett. **113**, 082502 (2014).
[10] K. G. Leach *et al.*, Nucl. Instrum. Methods Phys. Res., Sect. A **780**, 91 (2015).
[11] G. Li, R. Segel, N. D. Scielzo, P. F. Bertone, F. Buchinger, S. Caldwell, A. Chaudhuri, J. A. Clark, J. E. Crawford, C. M. Deibel, J. Fallis, S. Gulick, G. Gwinner, D. Lascar, A. F. Levand, M. Pedretti, G. Savard, K. S. Sharma, M. G. Sternberg, T. Sun, J. Van Schelt, R. M. Yee, and B. J. Zabransky, Phys. Rev. Lett. **110**, 092502 (2013).
[12] M. G. Sternberg, R. Segel, N. D. Scielzo, G. Savard, J. A. Clark, P. F. Bertone, F. Buchinger, M. Burkey, S. Caldwell, A. Chaudhuri, J. E. Crawford, C. M. Deibel, J. Greene, S. Gulick, D. Lascar, A. F. Levand, G. Li, A. Pérez Galván, K. S. Sharma, J. Van Schelt, R. M. Yee, and B. J. Zabransky, Phys. Rev. Lett. **115**, 182501 (2015).
[13] S. Caldwell, Ph.D. thesis, University of Chicago, 2015.
[14] A. Czeszumska, Ph.D. thesis, University of California, Berkeley, 2016.
[15] B. Fogelberg, B. Ekström, L. Sihver, and G. Rudstam, Phys. Rev. C **41**, R1890(R) (1990).
[16] A. A. Sonzogni, Nucl. Data Sheets **103**, 1 (2004).
[17] H. A. Weidenmüller, Rev. Mod. Phys. **33**, 574 (1961).
[18] E. K. Warburton, D. E. Alburger, and D. H. Wilkinson, Phys. Rev. C **26**, 1186 (1982).
[19] A. C. Hayes, J. L. Friar, G. T. Garvey, G. Jungman, and G. Jonkmans, Phys. Rev. Lett. **112**, 202501 (2014).
[20] D.-L. Fang and B. A. Brown, Phys. Rev. C **91**, 025503 (2015).
[21] E. K. Warburton and I. S. Towner, Phys. Lett. B **294**, 1 (1992).
[22] A. H. Snell and F. Pleasonton, Phys. Rev. **111**, 1338 (1958).
[23] K. Siegl *et al.* (unpublished).
[24] G. Savard *et al.*, Nucl. Instrum. Methods Phys. Res., Sect. B **266**, 4086 (2008).
[25] C. N. Davids and D. Peterson, Nucl. Instrum. Methods Phys. Res., Sect. B **266**, 4449 (2008).
[26] N. D. Scielzo *et al.*, Nucl. Instrum. Methods Phys. Res., Sect. A **681**, 94 (2012).
[27] M. Lampton and C. W. Carlson, Rev. Sci. Instrum. **50**, 1093 (1979).
[28] K. Furuya and Y. Hatano, Int. J. Mass Spectrom. **218**, 237 (2002).
[29] E. Lienard *et al.*, Nucl. Instrum. Methods Phys. Res., Sect. A **551**, 375 (2005).
[30] J. Oberheide, P. Wilhelms, and M. Zimmer, Meas. Sci. Technol. **8**, 351 (1997).
[31] G. W. Fraser, Int. J. Mass Spectrom. **215**, 13 (2002).
[32] N. D. Scielzo, S. J. Freedman, B. K. Fujikawa, and P. A. Vetter, Phys. Rev. A **68**, 022716 (2003).
[33] R. Capote *et al.*, Nucl. Data Sheets **110**, 3107 (2009).
[34] S. Agostinelli *et al.*, Nucl. Instrum. Methods Phys. Res., Sect. A **506**, 250 (2003).
[35] J. Allison *et al.*, IEEE Trans. Nucl. Sci. **53**, 270 (2006).
[36] J. Allison *et al.*, Nucl. Instrum. Methods Phys. Res., Sect. A **835**, 186 (2016).

[37] D. J. Manura and D. A. Dahl, Simion Version 8.0/8.1 User Manual (2011).
[38] T. A. Carlson, Phys. Rev. **131**, 676 (1963).
[39] A. H. Snell and F. Pleasonton, Phys. Rev. **107**, 740 (1957).
[40] T. A. Carlson, Phys. Rev. **129**, 2220 (1963).
[41] T. A. Carlson, Phys. Rev. **130**, 2361 (1963).
[42] M. Morita, Prog. Theor. Phys. **9**, 345 (1953).
[43] J.-I. Fujita, Phys. Rev. **126**, 202 (1962).
[44] J. C. Hardy *et al.*, Phys. Lett. B **71**, 307 (1977).
[45] A.-A. Zakari-Issoufou *et al.*, Phys. Rev. Lett. **115**, 102503 (2015).
[46] B. C. Rasco, M. Wolińska-Cichocka, A. Fijałkowska, K. P. Rykaczewski, M. Karny, R. K. Grzywacz, K. C. Goetz, C. J. Gross, D. W. Stracener, E. F. Zganjar, J. C. Batchelder, J. C. Blackmon, N. T. Brewer, S. Go, B. Heffron, T. King, J. T. Matta, K. Miernik, C. D. Nesaraja, S. V. Paulauskas, M. M. Rajabali, E. H. Wang, J. A. Winger, Y. Xiao, and C. J. Zachary, Phys. Rev. Lett. **117**, 092501 (2016).
[47] C. M. Baglin, Nucl. Data Sheets **113**, 2187 (2012).
[48] G. Savard *et al.*, Nucl. Instrum. Methods Phys. Res., Sect. B **376**, 246 (2016).
[49] T. Y. Hirsh *et al.*, Nucl. Instrum. Methods Phys. Res., Sect. B **376**, 229 (2016).